Micropatterned Structural Control Suppresses Mechanotaxis of Endothelial Cells

Xiefan Lin and Brian P. Helmke

Department of Biomedical Engineering and Robert M. Berne Cardiovascular Research Center, University of Virginia, Charlottesville, Virginia 22908

ABSTRACT Vascular endothelial cell migration is critical in many physiological processes including wound healing and stent endothelialization. To determine how preexisting cell morphology influences cell migration under fluid shear stress, endothelial cells were preset in an elongated morphology on micropatterned substrates, and unidirectional shear stress was applied either parallel or perpendicular to the cell elongation axis. On micropatterned 20-μm lines, cells exhibited an elongated morphology with stress fibers and focal adhesion sites aligned parallel to the lines. On 115-μm lines, cell morphology varied as a function of distance from the line edge. Unidirectional shear stress caused unpatterned cells in a confluent monolayer to exhibit triphasic mechanotaxis behavior. During the first 3 h, cell migration speed increased in a direction antiparallel to the shear stress direction. Migration speed then slowed and direction became spatially heterogeneous. Starting 11–12 h after the onset of shear stress, the unpatterned cells migrated primarily in the downstream direction, and migration speed increased significantly. In contrast, mechanotaxis was suppressed after the onset of shear stress in cells on micropatterned lines during the same time period, for the cases of both parallel and perpendicular flow. The directional persistence time was much longer for cells on the micropatterned lines, and it decreased significantly after flow onset. Migration trajectories were highly correlated among micropatterned cells within a three-cell neighborhood, and shear stress disrupted this spatially correlated migration behavior. Thus, presetting structural morphology may interfere with mechanisms of sensing local physical cues, which are critical for establishing mechanotaxis in response to hemodynamic shear stress.

INTRODUCTION

A grand challenge in cell biology and regenerative medicine is to understand and to control physiological mechanisms that regulate cell polarity and migration. An ability to engineer directional cell motility would open doors to novel therapeutic approaches in cancer, wound healing, and vascular biology. Regulation of cell polarity during migration involves the dynamic regulation of spatial and temporal events in the cytoplasm (1). A complex system of signaling networks balances the sensing of directional cues in the extracellular microenvironment with the remodeling of intracellular structure and transport processes. Recent advances in the understanding of directional cell migration under physiological applied mechanical forces, a process called mechanotaxis (2), add to the available toolbox for engineering cell behavior. However, the interplay between extracellular mechanochemical cues and preexisting cell structure to remodel directional polarity remains unclear.

Vascular endothelial cell (EC) migration under hemodynamic shear stress plays an important role in physiological and pathological processes such as microvascular remodeling (3) and reendothelialization after angioplasty and stent placement (4). In vitro, laminar shear stress enhances EC migration associated with wound closure (5,6). On average, ECs migrate preferentially in a direction parallel to that of unidirectional shear stress (6,7) and away from high spatial gradients of shear stress (8).

In confluent monolayers, as in vivo, ECs align their shape and structure parallel to the flow direction (9–11), including the reorganization of cell-cell junctions (12) and the elongation of focal adhesion sites (13). Paradoxically, EC motility within a confluent monolayer increases under unidirectional shear stress in a manner consistent with the remodeling of intercellular junctions, even though the net displacement of cells after 48 h of shear stress is negligible (8). Increased motility after adaptation to shear stress without a preferred direction of migration within the confluent monolayer contrasts with directional migration parallel to the shear stress direction in subconfluent layers of ECs (2). These observations pose a major challenge for engineering cell migration: Are morphological and structural dynamics only a passive readout of adaptation to extracellular applied force, or do they also actively govern cell functions such as directional migration?

In this study, the goal was to preset EC morphology to mimic that of a shear stress-adapted monolayer to separate the influence of preexisting cell structure from that of mechanoadaptation mechanisms on migration behavior. We used micropatterned lines of extracellular matrix to establish ECs in an elongated morphology and applied unidirectional laminar shear stress in the direction either parallel or perpendicular to the lines. The micropatterned lines provided an intervention to

Submitted December 12, 2007, and accepted for publication June 9, 2008.

Address reprint requests to Brian P. Helmke, PhD, Dept. of Biomedical Engineering, University of Virginia, PO Box 800759, Charlottesville, VA 22908. Tel.: 434-924-1726; Fax: 434-982-3870; E-mail: helmke@virginia.edu.

Editor: Gaudenz Danuser.

0006-3495/08/09/3066/13 $2.00

doi: 10.1529/biophysj.107.127761

investigate the interaction between the preexisting cell structure and the hemodynamic shear stress on the dynamics of cell migration and structural remodeling.

MATERIALS AND METHODS

Microcontact printing

The micropatterned surface of fibronectin was created by microcontact printing (14,15). Briefly, a silicon master pattern fabricated by photolithography was used to cast a poly(dimethylsiloxane) (PDMS) stamp (Sylgard 184, Dow Corning, Midland, MI) with a base/curing agent ratio of 10:1. Gold was sputtered onto cleaned coverslips (Lesker, Clairton, PA) to a thickness of ~12 nm. The PDMS stamp was inked with 2 mM 1-octadecanethiol (Aldrich, St. Louis, MO), blown dry with N_2 gas, and gently pressed against the gold-coated coverslip for ~20 s. The unprinted area was blocked with 2 mM tri(ethylene glycol)-terminated alkanethiol (ProChimia Surfaces, Sopot, Poland). After rinsing with phosphate-buffered saline, the surface was incubated with 30 μg ml^{-1} fibronectin for 2 h before cells were plated onto it.

Control unpatterned surfaces were fabricated by a similar method. Instead of stamping, 1-octadecanethiol solutions were washed onto the entire gold-coated coverslip surface for 20 s. Blocking and fibronectin incubation steps were then performed in an identical manner as for the microcontact printed coverslips.

Cell culture

Bovine aortic ECs (passage 11–15) were grown on the fibronectin surfaces in a humidified 5% CO_2 incubator at 37°C in complete growth medium consisting of Dulbecco's modified Eagle's medium (Gibco, Gaithersburg, MD) supplemented with 10% heat-inactivated newborn calf serum (HyClone, Logan, UT), 2.92 mg ml^{-1} L-glutamine (Gibco), and 1000 μg ml^{-1} penicillin-streptomycin (Gibco).

Shear flow experiment and image acquisition

Coverslips containing ECs were assembled aseptically into a parallel-plate flow chamber (FCS2, Bioptechs, Butler, PA) in a closed flow loop as described previously (16). Briefly, flow through the chamber was driven by gravity to create a wall shear stress of 1.5 Pa. Fluid from a warmed downstream reservoir was recirculated using a peristaltic pump. The temperature at the flow chamber was maintained at 37°C using a temperature controller (Bioptechs), and pH was maintained by equilibrating the medium with humidified 5% CO_2. Brightfield images were acquired in 5-min intervals using a DeltaVision RT microscope system (Applied Precision, Issaquah, WA).

Cell tracking and evaluation of methods

Time-lapse images were imported into ImageJ (17) or MATLAB (The Mathworks, Natick, MA) software for analysis. EC positions as a function of time were tracked in 6–9 different fields of view from three independent experiments.

A semiautomatic algorithm was designed in MATLAB to track EC migration on the unpatterned substrates. Contrast-enhanced brightfield images were thresholded to generate a binary image of cell objects. Cell boundaries were obtained by skeletonization and the removal of broken lines. Cell centroid positions were computed from each cell object boundary. Since the sampling rate was fast enough that cell displacement between two frames was much smaller than cell size, the centroid position for each individual cell object was considered to match in the subsequent frame with that which yielded the minimum displacement. Cell objects that did not correspond to a centroid location within one cell diameter in the subsequent frame were automatically removed.

The tracking algorithm was validated by analyzing error with respect to manual ''ground truth'' measurements. First, the centroid positions of 50 randomly picked cells in one frame were computed by manually outlining the cell boundary and comparing to the centroid positions derived by the algorithm. The average mean-square error was <1 pixel^2, indicating that position estimations by manual and automatic methods were comparable. Thus, analyses from manually and automatically tracked cells were compared from different experiments.

Analysis of cell migration

To analyze quantitatively the cell migration behavior in response to shear stress, ensemble-averaged values of instantaneous cell speed $\langle \text{Speed} \rangle$ and instantaneous velocity components ($\langle V_x \rangle$,$\langle V_y \rangle$) were computed as

$$\langle \text{Speed} \rangle = \frac{1}{N}\sum_{i=1}^{N}\sqrt{\left(\frac{x_i' - x_i}{\Delta t}\right)^2 + \left(\frac{y_i' - y_i}{\Delta t}\right)^2},$$

$$\langle V_x \rangle = \frac{1}{N}\sum_{i=1}^{N}\left(\frac{x_i' - x_i}{\Delta t}\right),$$

$$\langle V_y \rangle = \frac{1}{N}\sum_{i=1}^{N}\left(\frac{y_i' - y_i}{\Delta t}\right),$$

using the starting (x, y) and ending (x', y') positions of N cells during a given time interval (Δt). Average cell speed indicates the motility of the population, and the average projected velocities indicate the migration direction along the x and y axes. A zero average speed implies nonmotile cells, whereas a projected velocity near zero combined with a nonzero speed indicates that an equal number of cells are moving in opposite directions along the axis with similar speeds.

The direction of cell migration was analyzed using a nonparametric circular statistics approach (18). For cell migration orientation on unpatterned surfaces, velocity vector angles, mod(2π), were analyzed directly. Since cell migration orientation angles on the patterned lines fit a bimodal distribution, they were converted into unimodal data by doubling the orientation angles. The direction angles on horizontal lines were rotated $\pi/2$ onto the vertical axis before the doubling transformation. The vector angles

$$\theta_i = \tan^{-1}\left(\frac{y_i' - y_i}{x_i' - x_i}\right),$$

$i = 1, \ldots, N$, were used to compute mean orientation angle

$$\overline{\theta} = \begin{cases} \tan^{-1}(S/C) & S > 0,\ C > 0 \\ \tan^{-1}(S/C) + \pi & C < 0 \\ \tan^{-1}(S/C) + 2\pi & S < 0,\ C > 0 \end{cases},$$

where

$$C = \sum_{i=1}^{N}\cos\theta_i \quad \text{and} \quad S = \sum_{i=1}^{N}\sin\theta_i.$$

The first central trigonometric moment m_1 is the mean resultant length $\overline{R} = R/N$, which was computed from $R^2 = C^2 + S^2$. The second central trigonometric moment was computed as

$$m_2 = \frac{1}{N}\sum_{i=1}^{N}\cos 2(\theta_i - \overline{\theta}).$$

The sample circular dispersion and circular standard error were estimated by

$$\hat{\delta} = (1 - m_2)/2m_1^2 \quad \text{and} \quad \hat{\sigma}^2 = \hat{\delta}/N,$$

respectively. Finally, the $100(1 - \alpha/2)\%$ confidence interval around the mean orientation angle was then given by $(\overline{\theta} - \sin^{-1}(z_{\alpha/2}\hat{\sigma}), \quad \overline{\theta} + \sin^{-1}(z_{\alpha/2}\hat{\sigma}))$, where $z_{\alpha/2}$ is derived from the t distribution. A modified Rayleigh test (V-test) was used to compare mean orientation angles among test conditions at a significance level of $\alpha = 0.05$.

A temporal and spatial correlation analysis of cell migration trajectories was performed. To determine the temporal correlation patterns, a random walk model was used to calculate directional persistence time (P) and cell speed (S) (19) according to

$$\langle d^2(t)\rangle = 2S^2P\left[t - P(1 - e^{-t/P})\right],$$

where S is the root mean-squared speed, P is the directional persistence time, and $\langle d^2(t)\rangle$ is the mean-squared displacement. Both S and P provide measures of cell movement through time: S represents an average displacement rate, and P describes the time during which cell movement persists in the same direction. A nonoverlapping method was used to compute mean-square displacement from the cell centroid path according to previously described methods (20,21). Cell speed was computed by dividing root mean-squared displacement during the smallest time interval (20 min) by that interval. Directional persistence time was solved by curve-fitting using a nonlinear least-squares regression. Individual cell speed and directional persistence time were computed for each field of view in the unpatterned cell case and for each line in the micropatterned case. Results are presented as the average and standard error of P and S.

The spatial correlation among cell migration trajectories reveals how the migratory behavior of one cell was influenced by the neighboring cells. For the unpatterned monolayers, the correlation function was calculated between one cell and all the other cells in the same field of view using a previously described method (22). For the cells on the micropatterns, the cell migration trajectory for one cell was cross correlated with all the other cells on the same patterned line. Consider n cells on a patterned line with the trajectory of the ith cell ($i = 1, \ldots, n$) given by (x_{it},y_{it}), where $t = 1, \ldots, m$. Since the migration perpendicular to the lines was negligible, the migration trajectory was reduced to a one-dimensional analysis along the axis of the micropatterned line. The sample covariance between the position trajectories of the ith cell and the jth cell ($j = 1, \ldots, n - 1$) on a horizontal pattern is given by

$$S_{ij} = \sum_{t=1}^{m} x_{it}x_{jt} - \frac{1}{m}\sum_{t=1}^{m} x_{it}\sum_{t=1}^{m} x_{jt},$$

and the variance in the position of the ith cell is

$$S_{ii} = \frac{1}{m-1}\sum_{t=1}^{m} x_{it}^2 - \frac{m}{m-1}\left(\sum_{t=1}^{m} x_{it}\right)^2.$$

The covariance and variance for the cells on the vertical patterns were calculated similarly using y_{it}. Finally, the product moment correlation coefficient was computed for the ith and jth cell as

$$r_{ij} = \frac{S_{ij}}{\sqrt{S_{ii}}\sqrt{S_{jj}}}.$$

A zero cross correlation between migration trajectories of neighboring cells suggests that these cells move individually in different directions, whereas a value of r_{ij} approaching one indicates a pair of cells migrating in along nearly parallel trajectories. Therefore, the cross correlation analysis reveals locally correlated migration behavior among groups of adjacent cells. Since the sampling distribution of r_{ij} was not normal, a nonparametric statistical analysis was performed. The sign test was used to compute 95% confidence intervals, and the sign test and Kruskal-Wallis test were used to test for differences between median values at a 5% type I error rate.

RESULTS

Unidirectional shear stress induces multiphasic mechanotaxis of ECs in an unpatterned confluent monolayer

The migration behavior of ECs in an unpatterned confluent monolayer served as a physiological baseline during an interval from 4 h before to 16 h after the onset of unidirectional steady laminar shear stress (1.5 Pa). The following components of the ensemble-averaged velocity vector were analyzed as a function of time: magnitude of the velocity vector $\langle$Speed$\rangle$, orientation with respect to the x axis (θ), projected x-component $\langle V_x\rangle$, and projected y-component $\langle V_y\rangle$.

Under no-flow conditions, individual migration tracks clustered around the origin, with similar magnitude in all directions (Fig. 1 *A* and Supplementary Material, Movie S1, Data S1). The migration tracks were biased toward the left (upstream direction) during the first 4-h period after flow onset and became nondirectional again during 4–8 h after flow onset. The magnitude of the migration tracks was similar for the no-flow interval and the first two 4-h periods after flow onset but showed a significant increase during the 8–12-h and 12–16-h periods. In addition, during the 12–16-h period after flow onset, migration tracks exhibited significant bias toward the right (downstream direction).

A quantitative analysis of over >4000 cells showed that during the 4-h interval before the onset of shear stress, the speed of EC migration in confluent monolayers was ~0.1 μm min^{-1} (Fig. 1 *B*, time <0 h). The average migration velocity projected onto the x (Fig. 1 *C*) and y (Fig. 1 *D*) axes fluctuated around 0 μm min^{-1}, indicating that the number of cells migrating in opposite directions were approximately equal. After the onset of shear stress oriented parallel to the x axis, the cell migration behavior underwent a multiphase process. During the first ~3 h after the onset of shear stress, the migration speed increased, and $\langle V_x\rangle$ was negative, indicating that most cells migrated in the upstream direction against the shear stress. During a second phase after 3 h of shear stress, migration speed and $\langle V_x\rangle$ returned to values similar to those before the onset of shear stress. Finally, after ~11 h of shear stress, migration speed was significantly increased relative to no-flow values, and $\langle V_x\rangle$ was positive. Since $\langle V_y\rangle$ fluctuated around 0 μm min^{-1}, directional biases in migration rates perpendicular to the flow direction did not exist. Overall, these data suggest that ECs in a confluent monolayer initially migrate in the upstream direction during phase 1. Phase 2 represents a transitional period with decreased motility that allowed cells to reverse their migration direction. Finally, cell motility increases significantly in the downstream direction during phase 3 as they complete long-term adaptation to the shear stress.

Statistical analysis of circular histograms of migration velocity orientation clearly demonstrated multiphasic directional polarity in EC migration after the onset of shear stress (Fig. 1 *E*). Before the onset of shear stress (time <0 h), a

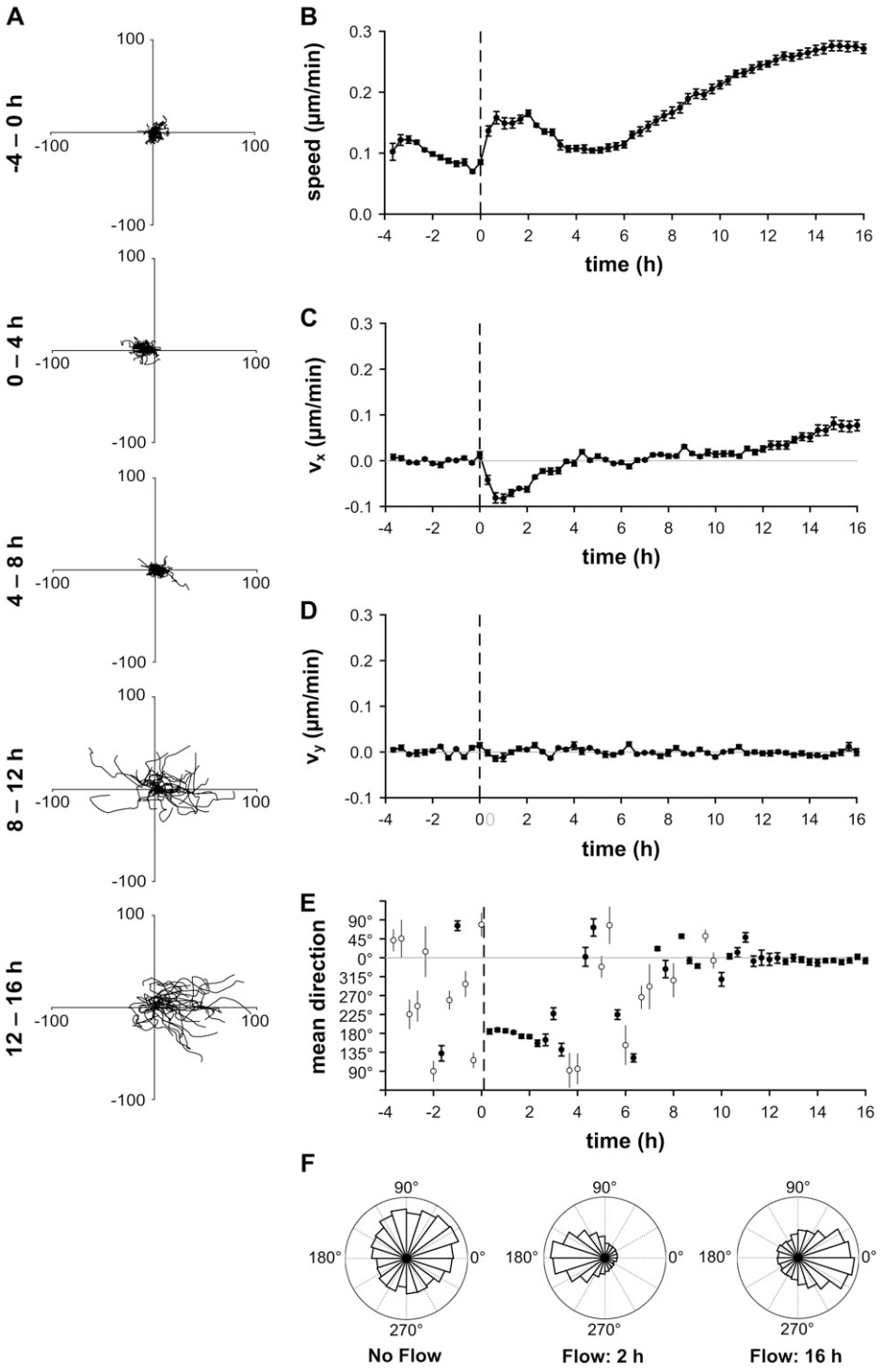

FIGURE 1 (*A*) Migration tracks for 30 representative ECs in an unpatterned confluent monolayer before (time <0 h) and after (time >0 h) flow onset. EC positions were measured every 20 min during 4-h intervals. Flow direction, left to right. (*B*) Mean migration speed ⟨Speed⟩, (*C*) mean velocity projected onto the horizontal axis $\langle V_x \rangle$, and (*D*) mean velocity projected onto the vertical axis $\langle V_y \rangle$ for unpatterned confluent EC layers before (time <0 h) and after (time >0 h) the onset of shear stress ($n = 9$ fields of view; error bars, standard error). (*E*) Mean direction of migration relative to the flow axis (0°). Closed symbols, mean is significant ($p < 0.05$, Rayleigh test); open symbols, directions are uniformly distributed ($n = 9$ fields of view; error bars, circular standard error). (*F*) Angular histograms of migration directions just before flow onset, 2 h after flow onset, and 16 h after flow onset.

unimodal mean orientation of cell migration was not significant at the 95% confidence level (Rayleigh test); i.e., cells migrated randomly in all directions. An example angular histogram just before the onset of shear stress shows a uniform distribution of migration directions (Fig. 1 *F*). During phase 1 (0–3 h) after the onset of shear stress (oriented at 0°), the mean velocity orientation was significantly clustered around 180° (Fig. 1 *E*, $p < 0.01$, V-test), and a circular histogram indicated that cells migrated preferentially opposite the shear stress direction (Fig. 1 *F*). Direction of migration again became random during phase 2. Finally, the mean velocity orientation was significantly clustered around 0° during phase 3 (11–16 h after the onset of shear stress, Fig. 1 *E*). An example circular histogram confirmed that cells migrated preferentially parallel to the direction of shear stress during this interval (Fig. 1 *F*).

Shear stress-induced mechanotaxis is suppressed in ECs on micropatterned lines

ECs on 20-μm-wide micropatterned lines were elongated in shape and aligned parallel to the direction of the lines (Supplementary Material, Fig. S1, Data S1). Patterned ECs contained thickened stress fiber bundles at cell edges, cytoplasmic stress fibers that were oriented primarily parallel to the major axis of cell elongation, and focal adhesions that were both elongated and aligned parallel to stress fibers. VE-cadherin was localized at the cell boundaries in between cells, similar to its distribution in confluent EC monolayers (Fig. S2, Data S1).

To determine whether elongated shape and structure influenced the ability of ECs to sense and adapt to unidirectional shear stress, the migration behavior of a quasiconfluent layer (based on number of cells per available adhesion area) of ECs on micropatterned lines was compared to that of unpatterned confluent monolayers. The line direction was positioned in acquired images either horizontally or vertically. When shear stress was applied from left to right, cells on the horizontal patterns experienced shear stress parallel to the morphological elongation, and cells on the vertical patterns experienced shear stress perpendicular to the elongation.

The migration tracks of micropatterned cells on horizontal lines (Fig. 2 *A* and Movie S2, Data S1) and on vertical lines (Fig. 3 *A*) demonstrated that micropatterned cells were migrating primarily along the pattern direction before flow onset. During the first 4 h after flow onset, the magnitude of migration tracks was dramatically decreased, and migration distance partially recovered in the following time periods.

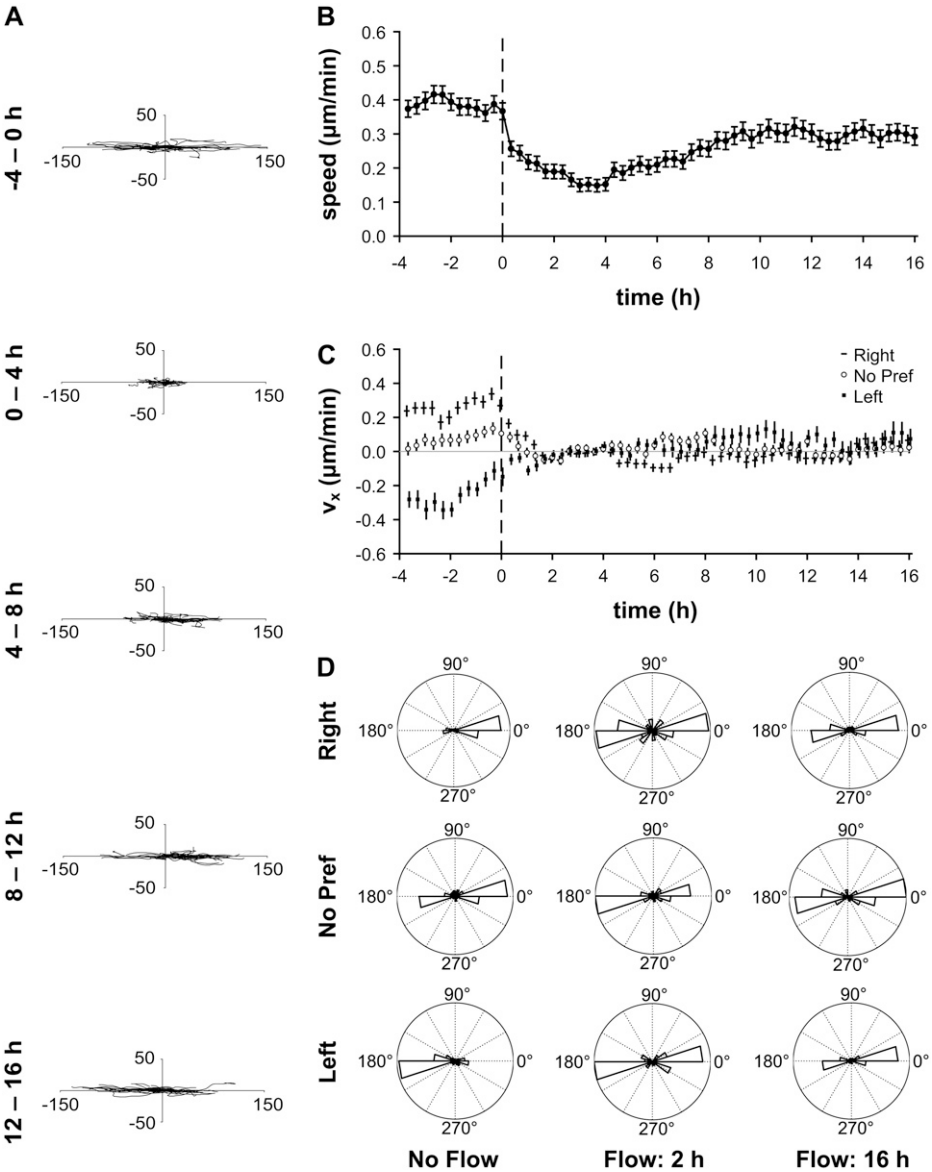

FIGURE 2 (*A*) Migration tracks for 30 representative ECs on 20-μm-wide horizontal lines before (time <0 h) and after (time >0 h) flow onset. EC positions were measured every 20 min during 4-h intervals. Flow direction, left to right. (*B*) Mean migration speed $\langle$Speed$\rangle$ of ECs on horizontal lines before (time <0 h) and after (time >0 h) the onset of shear stress (error bars, standard error). (*C*) Mean velocity projected onto the horizontal axis $\langle V_x \rangle$, grouped by mean direction before flow onset into left, right, and no preference. (*D*) Angular histograms of migration directions just before flow onset, 2 h after flow onset, and 16 h after flow onset.

Notably, equal numbers of cells migrated in the two directions along the micropatterns, and a preferential direction was never established by patterned cells under either parallel or perpendicular flow.

ECs on micropatterned lines exhibited obvious locally correlated migration behavior, which was characterized by cells on an individual patterned line migrating in the same direction. To investigate whether the initial migration direction influenced the ability of ECs in the group to sense and adapt to shear stress, micropatterned lines were categorized based on the circular distribution of overall cell migration directions time averaged for 4 h before the onset of shear stress. For example, horizontal lines were categorized as left, right, or no preference. The total ensemble-averaged total displacement during the 4-h interval before the onset of shear stress was normally distributed for all three cases, with a mean $\pm$ SD of -67 ± 63 μm, 63 ± 69 μm, and 19 ± 69 μm for the left, right, and no preference group, respectively. In a similar manner, cells on vertical lines were grouped into categories labeled up, down, and no preference.

Before the onset of shear stress parallel to the horizontal lines, cells migrated preferentially along the lines, and the migration speed in all three groups was significantly greater than that for cells in unpatterned confluent monolayers in the absence of shear stress (Fig. 2 *B*). The average *x*-component of velocity $\langle V_x \rangle$ indicated that most migration in the groups migrating left and right was parallel to the line axis (Fig. 2 *C*), since the average *y*-component of velocity $\langle V_y \rangle$ was not different from zero at any time point (analysis of variance (ANOVA), $p > 0.05$). In addition, the distribution of velocity vector orientations in the left and right groups under no-flow conditions clustered significantly around the micropatterned line axis (Fig. 2 *D*, V-test, $p < 0.001$). The no preference group contained cells migrating in both horizontal directions along the line under no-flow conditions (Fig. 2 *D*, Rayleigh test, $p > 0.05$); thus, $\langle V_x \rangle = 0$ for this group (Fig. 2 *C*). After the onset of shear stress, cell migration speed decreased significantly for all three groups and then gradually increased; however, even after 16 h of shear stress, ECs only partially recovered their initial migration speed. Interestingly, $\langle V_x \rangle$ in all three groups converged to zero after the onset of shear stress. Since average speed was nonzero, $\langle V_x \rangle = 0$ indicates that the onset of shear stress suppressed the directional migration of ECs, regardless of the original direction before flow. The angular distribution of velocity orientations indicated that equal numbers of cells were migrating in both directions along the micropatterned lines after the onset of shear stress (Fig. 2 *D*). Even after 16 h of shear stress, ECs did not reestablish a preferred direction of migration along the lines, in contrast to EC behavior in the unpatterned confluent monolayer.

Remarkably, ECs on vertical micropatterned lines oriented perpendicular to the shear stress direction exhibited a behavior nearly identical to that on horizontal lines. Before the onset of shear stress, the average migration speed was similar to that on horizontal lines and significantly greater than that in an unpatterned confluent monolayer (Fig. 3 *B*). The average x-component of velocity $\langle V_x \rangle$ was not different from zero (ANOVA, $p > 0.05$), and ECs migrated primarily along the vertical line direction. ECs migrating in the up or down directions exhibited similar velocities $\langle V_y \rangle$ as those on horizontal lines (Fig. 3 *C*), and lines containing ECs migrating in both directions along the line resulted in $\langle V_y \rangle = 0$. After the onset of shear stress, $\langle V_y \rangle$ converged to zero in all groups, indicating that ECs began to migrate in both directions without preference (Fig. 3 *D*) regardless of the initial preferred direction of migration.

To determine whether the preexisting cell structure or micropattern line width contributed to the suppression of the triphasic mechanotaxis response, migration tracks of ECs on 115-μm-wide horizontal lines were examined (Fig. 4). ECs along the centerline of these wider lines had polygonal shapes similar to those in unpatterned monolayers, whereas ECs near the edges were significantly elongated (Fig. S3, Data S1). Interestingly, ECs near the centerline exhibited triphasic mechanotaxis behavior (Fig. 4 *A*) similar to that in unpatterned confluent monolayers. Under no-flow conditions, ECs migrated in random directions, and migration was reoriented preferentially upstream during the first 4 h after the onset of shear stress parallel to the lines. Migration distance during the second 4-h interval was decreased and more randomly directed, and migration distance increased and was oriented primarily in the downstream direction in the interval 12–16 h after the onset of shear stress. Remarkably, elongated ECs near the edges of the same lines exhibited migration behavior similar to that on 20-μm lines instead of following the triphasic mechanotaxis of ECs near the centerline (Fig. 4 *B*). Migration direction was oriented primarily along the line edges before and after the onset of shear stress, even though migration away from the edge was physically possible. Migration distance was decreased initially after the onset of shear stress but recovered at later intervals. Thus, migration behavior on wider lines supported the hypothesis that preexisting cell structure is a primary determinant of the mechanotaxis responsiveness of ECs.

Shear stress suppresses correlated migration behavior on micropatterned substrates

After the onset of shear stress, the average cell velocity along micropatterned lines ($\langle V_x \rangle$ for horizontal line and $\langle V_y \rangle$ for vertical line) was near zero (Figs. 2 *C* and 3 *C*) and the distribution of average cell migration directions was equally divided in both directions along the line axes (Figs. 2 *D* and 3 *D*). A spatiotemporal correlation analysis was performed to determine whether this behavior was primarily the result of loss of locally correlated migration behavior or more frequent changes in direction.

Temporal correlation was analyzed by using a random walk model. In unpatterned confluent monolayers of cells, the av-

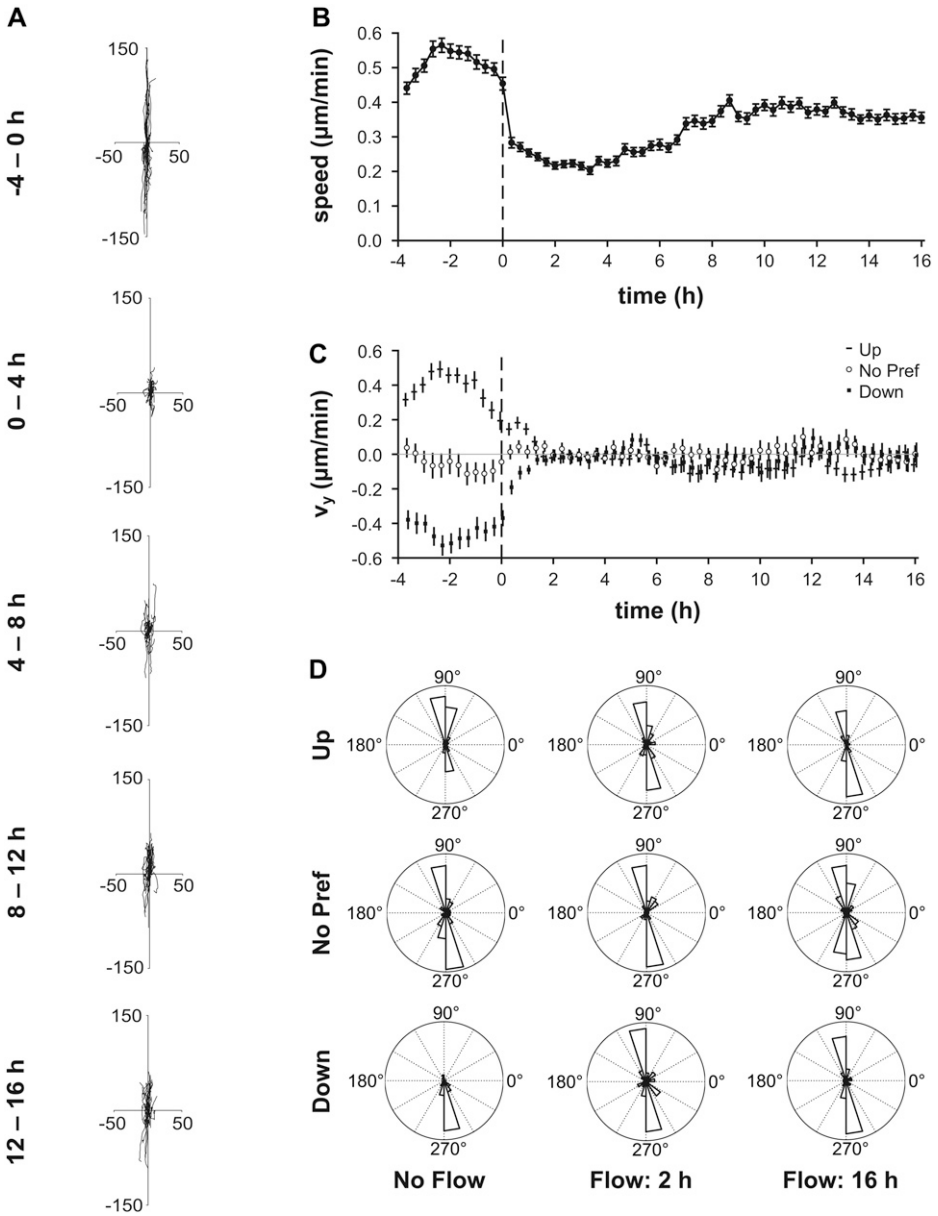

FIGURE 3 (*A*) Migration tracks for 30 representative ECs on 20-μm-wide vertical lines before (time <0 h) and after (time >0 h) flow onset. EC positions were measured every 20 min during 4-h intervals. Flow direction, left to right. (*B*) Mean migration speed $\langle$Speed$\rangle$ of ECs on vertical lines before (time <0 h) and after (time >0 h) the onset of shear stress (error bars, standard error). (*C*) Mean velocity projected onto the vertical axis $\langle V_y \rangle$, grouped by mean direction before flow onset into up, down, and no preference. (*D*) Angular histograms of migration directions just before flow onset, 2 h after flow onset, and 16 h after flow onset.

erage directional persistence time P before the onset of shear stress was 43 min (Fig. 5 *A*). P decreased slightly during the first 4-h interval after flow onset and decreased dramatically to 24 min during the interval from 4 h to 8 h after flow onset. This second interval corresponds to the transitional period (phase 2) when cells started to reverse their migration direction from upstream to downstream. In the next 4-h period (8–12 h), P recovered to 38 min. During the final interval 12–16 h after flow onset, as cells had already adapted their migration to the flow direction, directional persistence time increased to 51 min. Cell speed S was significantly greater for all four 4-h intervals in the presence of shear stress than before flow onset (Fig. 5 *B*). The triphasic trend after flow onset was similar to that in Fig. 1, although temporal averaging to compute S blunted the details. Cells on the horizontal micropatterns showed a fivefold increase in directional persistence time before flow onset (Fig. 5 *C*) compared to that of the unpatterned cells, indicating that the micropatterned lines caused cells to change their migration direction much less frequently. The onset of shear stress caused a significant decrease of persistence time during the 0–4-h and 4–8-h intervals after flow onset to a value similar to that of unpatterned cells. During the following intervals (8–12 h and 12–16 h), directional persistence time increased but did not fully recover to the value before the onset of shear stress. Cell speed also decreased significantly immediately after flow onset and only partially recovered during the 8–12-h and 12–16-h intervals (Fig. 5 *D*). The changes of directional persistence time and cell speed after flow were similar for cells on vertical cells (Fig. 5, *E* and *F*). Thus, cells on micropatterned lines reduce

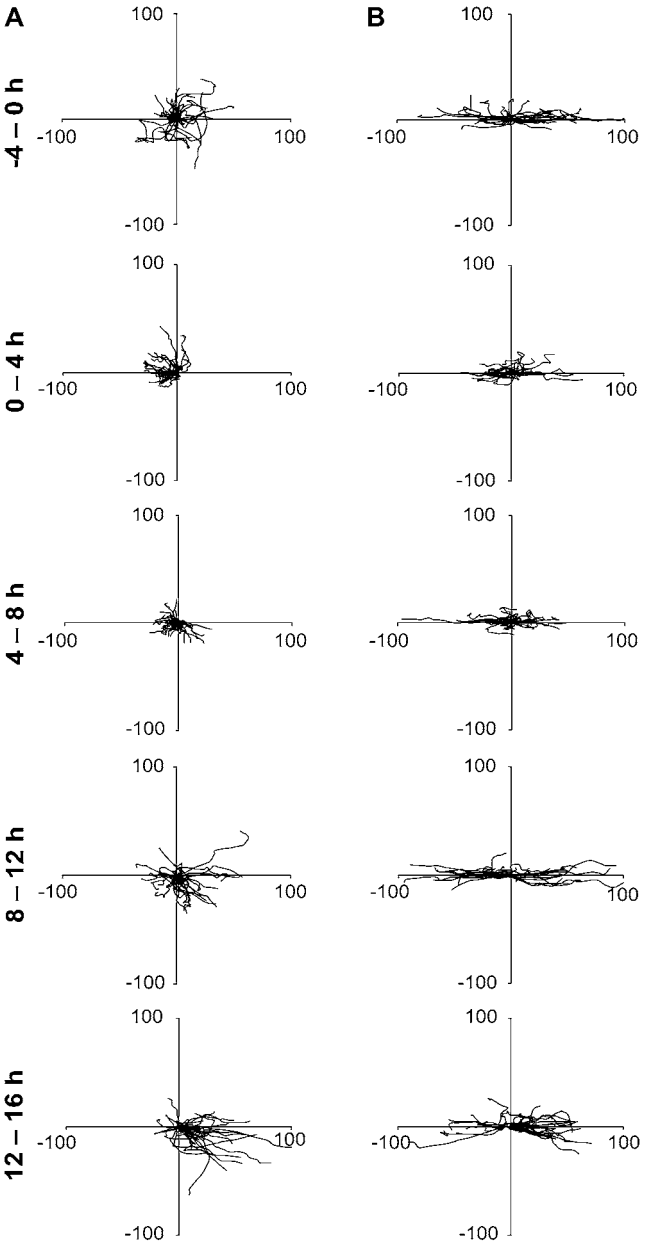

FIGURE 4 Migration tracks for 30 representative ECs located (*A*) at the centerline or (*B*) at the edges of 115-μm-wide horizontal lines before (time $<$0 h) and after (time $>$0 h) flow onset. EC positions were measured every 20 min during 4-h intervals. Flow direction, left to right.

their migration speed and change direction more frequently after the onset of shear stress, regardless of the shear stress direction relative to the major axis of cell elongation.

Both the temporal correlation analysis and the distinct patterns of $\langle V_x \rangle$ on the horizontal lines and $\langle V_y \rangle$ on the vertical lines suggested that cells on the same patterned line migrate preferentially in one direction before the onset of shear stress and that the coordinated migration patterns were disrupted after the onset of shear stress. To further investigate this locally correlated migration on the micropatterns, a spatial cross correlation analysis was performed among neighboring cell trajectories on the same patterned line during intervals 100 min before and 100 min after flow onset. Correlation coefficient values were computed as a function of separation distance between cell centroids (Fig. 6). The average separation distance between two adjacent cells was $\sim$30 μm on the patterned lines. Before the onset of shear stress, the migration of cells on horizontal patterns (Fig. 6 *A*) was highly correlated ($r_{ij} = 0.9$) to the migration of those within three cell distances (90 μm). The correlation coefficient decreased gradually as cell-cell distance increased and was not different from zero when the separation distance was larger than 390 μm.

Thus, the correlated migration behavior before the onset of shear stress was most significant among cells within a three-cell neighborhood, and cell migration was not affected by other cells more than 390 μm away. This highly correlated migration among cells within the three-cell neighborhood was specific for the micropatterned cells because migration trajectories were weakly correlated in unpatterned monolayers ($r_{ij} = 0.2$) even among closest neighbors within 30 μm. Thus, control of cell morphology or limitation of available adhesion area on micropatterned lines induced highly correlated cell migration for closely spaced cells. After the onset of shear stress, cell migration on the horizontal patterns was weakly correlated even among adjacent cells within a two-cell distance (60 μm) and uncorrelated among cells separated by more than 60 μm. A similar trend was observed for cells on vertical patterns (Fig. 6 *B*). The significant decrease of correlation coefficient after flow onset suggested the disruption of locally correlated migration by shear stress on the micropatterns, resulting in the convergence after flow onset of $\langle V_x \rangle$ on the horizontal lines and $\langle V_y \rangle$ on the vertical lines.

DISCUSSION

Occlusive coronary heart disease remains the highest cause of mortality in the United States (23), in part because of high rates of bypass graft failure (24) and delayed thrombosis after implant of either drug-eluting or bare metal stents (25,26). A critical unsolved problem is how to promote reendothelialization and to restore physiological endothelial function over the long term. Both bypass grafting and stent placement are predicted to introduce local disturbances to the hemodynamic flow field (27), which is already likely to represent a proatherogenic profile of reduced magnitude and amplified spatial and temporal gradients of shear stress (28). At these locations, the local shear stress profile has been implicated in disturbing major functions of the endothelium, including cell motility, apoptosis, proliferation, and contact inhibition (12,29). A first step toward improving endothelial wound healing after vascular interventions requires the determination of how cell migration and structural dynamics depend on interactions between local physical cues and hemodynamic shear stress profiles.

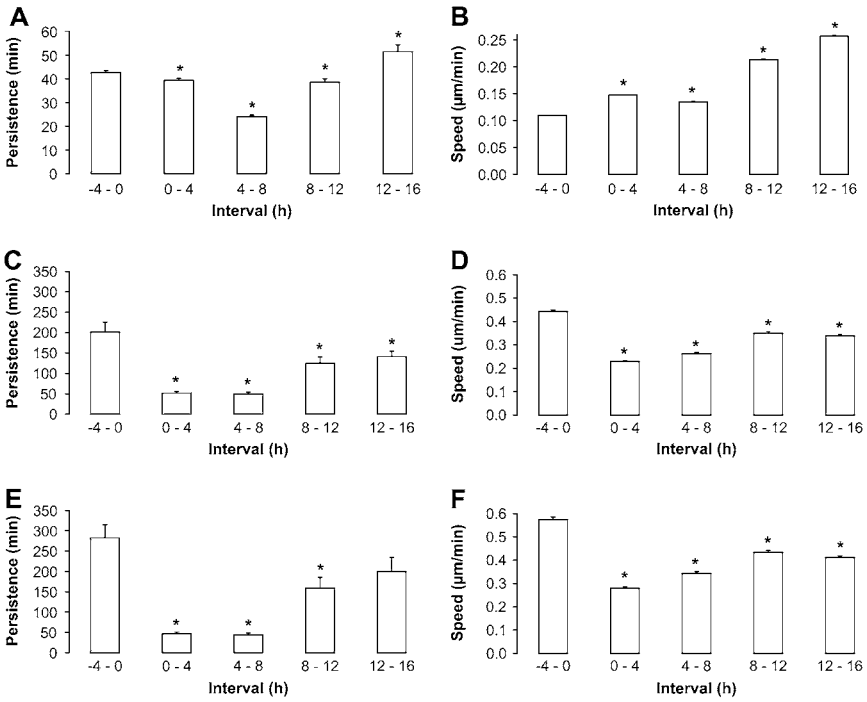

FIGURE 5 (*A*) Directional persistence time and (*B*) cell speed for unpatterned cells ($n = 9$ fields of view from three independent experiments). (*C*) Directional persistence time and (*D*) cell speed for cells on horizontal micropatterns ($n = 22$ micropatterned lines from three independent experiments). (*E*) Directional persistence time and (*F*) cell speed for cells on vertical micropatterns ($n = 19$ micropatterned lines from three independent experiments). Error bars, standard error. *Mean value significantly different from value during the no-flow interval ($p < 0.05$, ANOVA).

This study reports that preexisting EC structure modulates the mechanotaxis response to hemodynamic shear stress. In unpatterned confluent monolayers, ECs initially migrated in the upstream direction after the onset of shear stress. After a transitional period characterized by a decreased speed and a near zero average velocity, cells increased their migration speed in the downstream direction on a timescale that was consistent with adaptation to shear stress (>11 h). Measurements of the triphasic mechanotaxis response are derived directly from continuous tracking of living ECs migrating in a confluent monolayer. Previous studies have reported the reorganization of cytoskeleton and centrosome positions in cells fixed at discrete time points during adaptation to unidirectional steady shear stress (10). After 3 h of flow, actin-dense peripheral band content increased, and focal adhesions translocated toward the cell periphery. After 6 h, dense peripheral bands were absent, and the percentage of ECs with centrosomes located in the downstream half of the cell was decreased significantly.

After 12–24 h, cell shapes were elongated, and the percentage of cells with centrosomes in the downstream half returned to baseline (10) or increased (30). Although these three phases of remodeling were described as a ''triphasic'' response ''consistent with motility'' (10), cell motility was not measured directly since ECs were fixed and immunostained. More recent statistical approaches describe the spatial organization of intracellular compartments that are associated with planar cell polarity in single cells on micropatterned islands shaped like migrating cells (31). However, direct measurement of the triphasic mechanotaxis response in confluent EC monolayers has not previously been reported, and the mechanisms that determine directional polarity in a confluent monolayer of living cells remain poorly understood. Surprisingly, elongated ECs on micropatterned lines did not exhibit a similar triphasic pattern of migration after the onset of shear stress. Instead, they showed decreased motility and migrated similarly in both directions along the lines, regardless of the flow direction. Furthermore, both the spatial and temporal correlation patterns among cell migration trajectories on micropatterned lines were disrupted by shear stress.

Why would structural morphology in elongated cells suppress the dynamic mechanotaxis response to the onset of shear stress? Since alignment of actin stress fibers and focal adhesions in ECs on 20-μm micropatterned lines did not change after the onset of either parallel or perpendicular flow, it is reasonable to hypothesize that constant maintenance of elongated cell morphology and aligned structure is critical in suppressing mechanotaxis under flow. This idea is supported by the differential behavior of ECs on 115-μm-wide lines (Fig. 4). Mechanotaxis was suppressed in elongated cells near the line edges, even though ECs within a few cell diameters exhibited the triphasic behavior. If the micropattern-mediated restriction of cell morphology were to be released, directional mechanotaxis behavior would be expected to return. In fact, when ECs on lines perpendicular to the shear stress direction migrated off-pattern (in experiments in which the blocking of nonspecific protein adsorption failed), they first extended their lamellipodia to the off-pattern area and changed their shape away from the elongated morphology before they began to migrate in the direction of applied shear stress (data not shown). These cells migrated a greater dis-

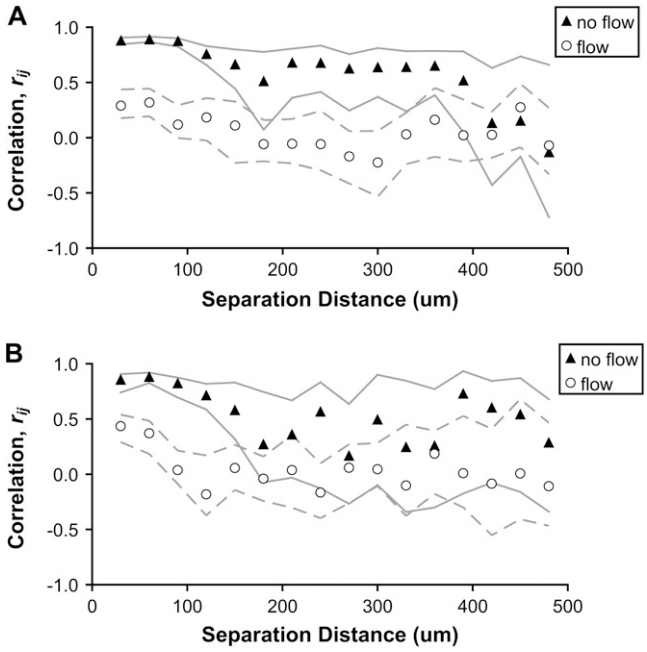

FIGURE 6 Cross correlation coefficient on (*A*) horizontal micropatterns and (*B*) vertical micropatterns. Black triangles and open dots represent median cross correlation coefficient before and after flow onset, respectively. Solid and dashed gray lines represent 95% confidence intervals of the median. The cross correlation coefficient was computed for each pair of cells on the same patterned line for a total of 21 horizontal lines and 19 vertical lines.

tance downstream than upstream, indicating that mechanotaxis was restored when the restriction of cell structure was released. Thus, mechanotaxis and structural adaptation are not mutually independent processes; interference with cell morphology and structure by micropatterning abrogates the mechanotaxis response.

Another possible explanation for the behavior of cells on micropatterned lines is that the triphasic mechanotaxis behavior is delayed rather than disrupted. However, several pieces of evidence argue against this hypothesis. In unpatterned confluent monolayers, ensemble-averaged cell speed did not decrease below the no-flow value at any time after flow onset, including during phase 2 remodeling and reorientation. In contrast, the average migration speed of micropatterned cells immediately decreased after flow onset, suggesting the disruption of mechanisms that determine motility characteristics. Furthermore, micropatterned cells did not exhibit coordinated directionality of migration at any time after the onset of flow, even though motility and persistence time of individual cells partially recovered after 16 h of flow. Thus, the suppression of mechanotaxis by presetting and maintaining the elongated cell structure pointed toward a mechanism of flow-induced migration response that was different from that of the unpatterned cells, which responded immediately to flow by migrating upstream. We speculate that even after longer periods of flow, mechanotaxis will not resume as long as the preset structure is maintained. Unfortunately, a technical limitation of the micropatterning approach is that ECs began to migrate off the patterns after more than 16 h of shear stress, even though cells remained confined to the patterns for ~2 weeks in the absence of flow. As a result, this hypothesis could not be tested directly.

Most previous studies on cell migration under fluid shear stress examined only single ECs, which exhibited immediate mechanotaxis in the downstream direction within 30 min (2). In contrast, the triphasic migration of ECs in unpatterned confluent monolayers suggested a contribution of cell-cell interactions to migration behavior. Furthermore, ECs on an individual micropatterned line exhibited locally correlated migration behavior that is consistent with intercellular communication. Before the onset of shear stress, migration trajectories were highly correlated among cells that were within a three-cell distance, and the correlation decreased with increased cell separation distance (Fig. 6). Migration trajectories remained correlated among cells that were separated by up to a 10-cell distance. The highly correlated migration was strongly suppressed by shear stress. Trajectories were only weakly correlated among neighboring cells within a two-cell distance, and trajectories became uncorrelated for larger separation distances. To our knowledge, these are the first measurements of a shear stress effect on the locally correlated migration behavior of cells on patterned lines. Interestingly, a similar effect of shear stress on functional gap junctional intercellular communication (GJIC) in confluent monolayers was recently measured (32). Before flow onset, a microinjected gap junction permeable dye was passed to 38 adjacent neighbors, corresponding to a distance of six to seven cell diameters. After 5 h of unidirectional shear stress, the dye reached only seven neighboring cells, a two-cell distance.

The decrease in GJIC with flow was similar to the decreased separation distance of correlated migration trajectories measured in this study. In addition, unpatterned confluent cells have been reported to undergo partial disassembly of adherens junctions during adaptation to flow (12). Consistent with the idea of differences in physical junction communication between unpatterned and patterned ECs, transient defects in the monolayer occasionally begin to appear during the second phase of transition to downstream migration after the onset of shear stress (Movie S1, Data S1), demonstrating the need to account for the role of cell-cell contact in mechanotaxis. However, the mechanism of increased motility cannot be due only to loss of cell contacts. High motility can occur even in the presence of intact tight and adherens junctions (33), and increased migration speed in the upstream direction during the first phase of mechanotaxis occurs before a significant increase in cell edge dynamics and transient defect formation that might suggest that loss of junctions occurred. Second, intercellular junctions reassemble stably after adaptation to shear stress (12) on the same timescale as increased downstream migration. Finally, locally correlated migration of ECs on 20-μm lines decreased after the onset of shear stress even though transient defects in cell-cell contact

were not visible in time-lapse movies (Movie S2, Data S1). Thus, shear stress-induced remodeling rather than loss of cell-cell junctions may be responsible for the loss of EC locally correlated migration behavior after flow onset.

The directional persistence time for unpatterned confluent EC monolayers before flow onset was similar to that reported previously (34,35). Blackman et al. reported an increase in directional persistence time to 140 min during a 24-h interval of steady unidirectional shear stress. The decreased persistence time reported here at a higher time resolution (every 4 h) reveals a faster dynamic behavior that corresponds to a triphasic migration pattern. During phase 3 (12–16 h after flow onset), persistence time increased significantly compared to that computed under no-flow conditions; so the increased directional persistence computed over a 24-h window is expected to be consistent with that reported by Blackman et al. Comparison of Fig. 1 *B* to Fig. 5 *B* further illustrates the effect of temporal averaging to compute *S*.

The triphasic profile of cell speed after flow onset is revealed in the analysis of migration trajectories (Fig. 1) but is less apparent when computed in 4-h windows in the persistence model (Fig. 5 *B*). The increase of persistence time on the patterned lines indicates that controlling the cell structure or limiting the available adhesion area altered the intrinsic migratory properties of those cells. Stabilization of lamellipodial protrusion has been shown to be associated with directional persistence in the migration of Chinese hamster ovary cells treated with epithelial growth factor (21). On the micropatterned lines, lamellipodial protrusion was observed in response to flow onset both at the ends and the sides of the elongated cells. However, stabilization of lamellipodial protrusion happened only at the ends (data not shown). Whether this spatially selective stabilization of lamellipodial protrusion is guided by the elongated and aligned cell structure remains to be investigated.

Interestingly, these measurements suggest that micropatterned ECs exhibit several behaviors that are similar to ECs in a confluent monolayer after adaptation to atheroprotective shear stress profiles. The cell density per available adhesion area on micropatterned lines was $>10^5$ cells cm^{-2}, which is similar to the density of ECs in a contact-inhibited unpatterned confluent monolayer, and both the cytoskeleton and focal adhesions exhibited morphologies similar to those in flow-adapted EC monolayers (10,36). Although restriction of cell spreading on micropatterned substrates may increase apoptosis (14), shear prevents cell loss (37). During the 20 h of cell tracking in unpatterned monolayers, 0.2% $\pm$ 0.1% of cells divided, and 1.8% $\pm$ 0.4% of cells were lost. In micropatterned layers, 1.4% $\pm$ 1.0% of cells divided, and 1.4% $\pm$ 1.3% of cells were lost. Thus, the change in the number of cells per area on both substrates was negligible, and cell loss could not account for differences in motility behavior. VE-cadherin in micropatterned cells was organized along cell-cell borders (Fig. S2, Data S1), similar to that of cells in unpatterned confluent monolayers. Both the shape index and orientation angle of the micropatterned cells were similar to those of the flow-adapted confluent monolayer (11). ECs exhibited an obvious locally correlated behavior in migration direction before flow onset, suggesting that planar cell polarity established by structural elongation promotes directional migration, similar to mechanisms that have been proposed for ECs in confluent monolayers after adaptation to shear stress (29).

Gene expression and signaling pathways can be set to a ''physiological baseline'' by shear stress preconditioning. For example, after preconditioning, changes in the expression of a number of shear-responsive genes are amplified after a secondary step increase in shear stress (38). Determining whether similar preconditioning effects exist for structural dynamics and cell motility remains unsolved, since preconditioning an EC monolayer to shear stress eliminates the possibility of investigating mechanotransmission in response to de novo force application. Therefore, micropatterned substrates provide a new toolset to directly investigate how preexisting cell structure modulates mechanisms of mechanosensing. The rapid decrease in the migration speed of micropatterned ECs after the onset of shear stress indicates that additional mechanical stabilization of the EC monolayer occurs even though cell structure appears similar to cells that have already adapted structurally to shear stress.

Thus, the investigation of mechanotransduction in flow-preconditioned ECs may not accurately reveal responses that are specific to mechanotransmission through cell structure, suggesting that mechanoadaptation to shear stress corresponds to a desensitization of mechanotransduction mechanisms. The idea of mechanodesensitization has been reported in other cell types, such as bone and neurons (39,40), and ECs may share similar mechanisms. ECs would be expected to exhibit similar mechanotaxis behaviors under nonreversing pulsatile flow as under steady unidirectional flow (41). Reversing oscillatory flow may disrupt the triphasic mechanotaxis of behavior in unpatterned confluent monolayers, since transient disruption of adherens and gap junctions occurs on a similar timescale. Since cell structure was demonstrated to be critical in determining migration behavior, the migration behavior of micropatterned cells may be insensitive to the flow profile if the mechanoadaptation response is desensitized by presetting ECs to an elongated structure.

In contrast to ECs after shear stress preconditioning, the preexisting cell structure in these experiments is determined primarily by the geometry of physical cues presented on micropatterned substrates (31). A tempting hypothesis is that substrate micropatterning serves as a substitute for adaptation or preconditioning to shear stress, based on similarities in cell structure and motility. However, several pieces of evidence argue against this hypothesis. ECs on a micropatterned haptotactic gradient of collagen extracellular matrix migrate in the direction of shear stress that is oriented perpendicularly to the collagen gradient (42), but only if the shear stress magnitude exceeds 0.2 Pa. In addition, a shear stress mag-

nitude of 1.2 Pa protects ECs on micropatterned lines of fibronectin against geometrically induced apoptosis (37). Consistent with other measurements in single cells, cell survival is attributed to shear stress-mediated activation of the small GTPase RhoA, recruitment and phosphorylation of focal adhesion kinase, and maturation of focal adhesion sites and stress fibers. When these data are considered together with shear stress-induced modulation of cell motility on micropatterned lines, a better hypothesis is that the preexisting cell structure is not sufficient for atheroprotection; adaptation to shear stress is still required. Future studies can now carefully interrogate cross talk between cell structure and mechanosensing mechanisms by using micropatterned substrates to specify structural configurations that may serve to sensitize intracellular mechanotransduction networks.

The suppression of mechanotaxis on micropatterned lines independent of the orientation with respect to the shear stress direction represents one example of a new cross talk behavior that must be solved. This study reveals new insights and challenges in understanding endothelial mechanotransmission and mechanotransduction. An important direction for the field is the elucidation of how cell-substrate interactions guide not just the adhesion but also the structural dynamics involved in mechanoadaptation. For example, the design of biomaterials for vascular stents or tissue-engineered vascular grafts must now consider cross talk between local physical cues and hemodynamic profiles to improve endothelial healing. Thus, the integration of bioengineering, materials science, and cell biology will open new avenues for clinical success involving mechanotherapy along with pharmacological approaches.

SUPPLEMENTARY MATERIAL

To view all of the supplemental files associated with this article, visit www.biophysj.org.

This study was supported by National Science Foundation Materials Research Science and Engineering Center for Nanoscopic Materials Design (DMR-0080016) and by National Institutes of Health grant HL-071958.

REFERENCES

1. Ridley, A. J., M. A. Schwartz, K. Burridge, R. A. Firtel, M. H. Ginsberg, G. Borisy, J. T. Parsons, and A. R. Horwitz. 2003. Cell migration: integrating signals from front to back. *Science*. 302:1704–1709.
2. Li, S., P. J. Butler, Y. Wang, Y. Hu, D. C. Han, S. Usami, J.-L. Guan, and S. Chien. 2002. The role of the dynamics of focal adhesion kinase in the mechanotaxis of endothelial cells. *Proc. Natl. Acad. Sci. USA*. 99:3546–3551.
3. Skalak, T. C., and R. J. Price. 1996. The role of mechanical stresses in microvascular remodeling. *Microcirculation*. 3:143–165.
4. Sprague, E. A., J. Luo, and J. C. Palmaz. 1997. Human aortic endothelial cell migration onto stent surfaces under static and flow conditions. *J. Vasc. Interv. Radiol*. 8:83–92.
5. Albuquerque, M. L. C., C. M. Waters, U. Savla, H. W. Schnaper, and A. S. Flozak. 2000. Shear stress enhances human endothelial cell wound closure in vitro. *Am. J. Physiol*. 279:H293–H302.
6. Hsu, P.-P., S. Li, Y.-S. Li, S. Usami, A. Ratcliffe, X. Wang, and S. Chien. 2001. Effects of flow patterns on endothelial cell migration into a zone of mechanical denudation. *Biochem. Biophys. Res. Commun*. 285:751–759.
7. Masuda, M., and K. Fujiwara. 1993. The biased lamellipodium development and microtubule organizing center position in vascular endothelial cells migrating under the influence of fluid flow. *Biol. Cell*. 77:237–245.
8. Tardy, Y., N. Resnick, T. Nagel, M. A. Gimbrone Jr., and C. F. Dewey Jr. 1997. Shear stress gradients remodel endothelial monolayers in vitro via a cell proliferation-migration-loss cycle. *Arterioscler. Thromb. Vasc. Biol*. 17:3102–3106.
9. Dewey, C. F. Jr., S. R. Bussolari, M. A. Gimbrone Jr., and P. F. Davies. 1981. The dynamic response of vascular endothelial cells to fluid shear stress. *J. Biomech. Eng*. 103:177–188.
10. Galbraith, C. G., R. Skalak, and S. Chien. 1998. Shear stress induces spatial reorganization of the endothelial cell cytoskeleton. *Cell Motil. Cytoskeleton*. 40:317–330.
11. Levesque, M. J., and R. M. Nerem. 1985. The elongation and orientation of cultured endothelial cells in response to shear stress. *J. Biomech. Eng*. 107:341–347.
12. Noria, S., D. B. Cowan, A. I. Gotlieb, and B. L. Langille. 1999. Transient and steady-state effects of shear stress on endothelial cell adherens junctions. *Circ. Res*. 85:504–514.
13. Davies, P. F., A. Robotewskyj, and M. L. Griem. 1994. Quantitative studies of endothelial cell adhesion: directional remodeling of focal adhesion sites in response to flow forces. *J. Clin. Invest*. 93:2031–2038.
14. Chen, C. S., M. Mrksich, S. Huang, G. M. Whitesides, and D. E. Ingber. 1997. Geometric control of cell life and death. *Science*. 276: 1425–1428.
15. Whitesides, G. M., E. Ostuni, S. Takayama, X. Jiang, and D. E. Ingber. 2001. Soft lithography in biology and biochemistry. *Annu. Rev. Biomed. Eng*. 3:335–373.
16. Helmke, B. P., R. D. Goldman, and P. F. Davies. 2000. Rapid displacement of vimentin intermediate filaments in living endothelial cells exposed to flow. *Circ. Res*. 86:745–752.
17. Abramoff, M. D., P. J. Magelhaes, and S. J. Ram. 2004. Image processing with ImageJ. *Biophotonics Intl*. 11:36–42.
18. Fisher, N. I. 1993. Statistical Analysis of Circular Data. Cambridge University Press, Cambridge, UK.
19. Dunn, G. A. 1983. Characterising a kinesis response: time averaged measures of cell speed and directional persistence. *Agents Actions Suppl*. 12:14–33.
20. Dickinson, R. B., and R. T. Tranquillo. 1993. Optimal estimation of cell movement indices from the statistical analysis of cell tracking data. *AIChE J*. 39:1995–2010.
21. Harms, B. D., G. M. Bassi, A. R. Horwitz, and D. A. Lauffenburger. 2005. Directional persistence of EGF-induced cell migration is associated with stabilization of lamellipodial protrusions. *Biophys. J*. 88: 1479–1488.
22. Weeks, E. R., J. C. Crocker, and D. A. Weitz. 2007. Short- and long-range correlated motion observed in colloidal glasses and liquids. *J. Phys. Condens. Matter*. 19:205131.
23. American Heart Association. 2007. Heart Disease and Stroke Statistics—2007 Update. American Heart Association, Dallas, TX.
24. Yusuf, S., S. Reddy, S. Ounpuu, and S. Anand. 2001. Global burden of cardiovascular diseases: part I: general considerations, the epidemiologic transition, risk factors, and impact of urbanization. *Circulation*. 104:2746–2753.
25. Joner, M., A. V. Finn, A. Farb, E. K. Mont, F. D. Kolodgie, E. Ladich, R. Kutys, K. Skorija, H. K. Gold, and R. Virmani. 2006. Pathology of drug-eluting stents in humans: delayed healing and late thrombotic risk. *J. Am. Coll. Cardiol*. 48:193–202.
26. Stankovic, G., J. Cosgrave, A. Chieffo, I. Iakovou, G. Sangiorgi, M. Montorfano, F. Airoldi, M. Carlino, I. Michev, L. Finci, and A. Colombo. 2006. Impact of sirolimus-eluting and paclitaxel-eluting

stents on outcome in patients with diabetes mellitus and stenting in more than one coronary artery. *Am. J. Cardiol.* 98:362–366.

27. LaDisa, J. F., I. Guler, L. E. Olson, D. A. Hettrick, J. R. Kersten, D. C. Warltier, and P. S. Pagel. 2003. Three-dimensional computational fluid dynamics modeling of alterations in coronary wall shear stress produced by stent implantation. *Ann. Biomed. Eng.* 31:972–980.
28. Ross, R. 1999. Atherosclerosis—an inflammatory disease. *N. Engl. J. Med.* 340:115–126.
29. McCue, S., D. Dajnowiec, F. Xu, M. Zhang, M. R. Jackson, and B. L. Langille. 2006. Shear stress regulates forward and reverse planar cell polarity of vascular endothelium in vivo and in vitro. *Circ. Res.* 98:939–946.
30. Tzima, E., W. B. Kiosses, M. A. del Pozo, and M. A. Schwartz. 2003. Localized cdc42 activation, detected using a novel assay, mediates microtubule organizing center positioning in endothelial cells in response to fluid shear stress. *J. Biol. Chem.* 278:31020–31023.
31. Thery, M., V. Racine, M. Piel, A. Pepin, A. Dimitrov, Y. Chen, J.-B. Sibarita, and M. Bornens. 2006. Anisotropy of cell adhesive microenvironment governs cell internal organization and orientation of polarity. *Proc. Natl. Acad. Sci. USA.* 103:19771–19776.
32. DePaola, N., P. F. Davies, W. F. Pritchard Jr., L. Florez, N. Harbeck, and D. C. Polacek. 1999. Spatial and temporal regulation of gap junction connexin43 in vascular endothelial cells exposed to controlled disturbed flows in vitro. *Proc. Natl. Acad. Sci. USA.* 96:3154–3159.
33. Guo, R., H. Sakamoto, S. Sugiura, and M. Ogawa. 2007. Endothelial cell motility is compatible with junctional integrity. *J. Cell. Physiol.* 211:327–335.
34. Blackman, B. R., G. Garcia-Cardena, and M. A. Gimbrone Jr. 2002. A new in vitro model to evaluate differential responses of endothelial cells to simulated arterial shear stress waveforms. *J. Biomech. Eng.* 124:397–407.
35. Simmers, M. B., A. W. Pryor, and B. R. Blackman. 2007. Arterial shear stress regulates endothelial cell-directed migration, polarity, and morphology in confluent monolayers. *Am. J. Physiol.* 293:H1937–H1946.
36. Wernick, M. N., M. L. Griem, A. Robotewskyj, and P. F. Davies. 1998. Image analysis of the dynamic changes of adhesion sites in endothelial cells subjected to directional flow in vitro. *J. Vasc. Invest.* 4:15–23.
37. Wu, C.-C., Y.-S. Li, J. H. Haga, R. Kaunas, J.-J. Chiu, F.-C. Su, S. Usami, and S. Chien. 2007. Directional shear flow and Rho activation prevent the endothelial cell apoptosis induced by micropatterned anisotropic geometry. *Proc. Natl. Acad. Sci. USA.* 104:1254–1259.
38. Passerini, A. G., A. Milsted, and S. E. Rittgers. 2003. Shear stress magnitude and directionality modulate growth factor gene expression in preconditioned vascular endothelial cells. *J. Vasc. Surg.* 37:182–190.
39. Cuche, G., S. Blat, and C. H. Malbert. 2001. Desensitization of ileal vagal receptors by short-chain fatty acids in pigs. *Am. J. Physiol.* 280:G1013–G1021.
40. Robling, A. G., D. B. Burr, and C. H. Turner. 2001. Recovery periods restore mechanosensitivity to dynamically loaded bone. *J. Exp. Biol.* 204:3389–3399.
41. Helmlinger, G., R. V. Geiger, S. Schreck, and R. M. Nerem. 1991. Effects of pulsatile flow on cultured vascular endothelial cell morphology. *J. Biomech. Eng.* 113:123–131.
42. Hsu, S., R. Thakar, D. Liepmann, and S. Li. 2005. Effects of shear stress on endothelial cell haptotaxis on micropatterned surfaces. *Biochem. Biophys. Res. Commun.* 337:401–409.